Turk J Elec Eng & Comp Sci, Vol.19, No.1, 2011, © TÜBİTAK
doi:10.3906/elk-1003-404

Stray magnetic field distributed around a PMSM

Ali Ahmed ADAM[1], Kayhan GÜLEZ[2], Selim KÖROĞLU[3]
[1]*Department of Electrical-Electronics Engineering, Engineering Faculty, Fatih University, İstanbul-TURKEY*
e-mail: aliadam@fatih.edu.tr
[2]*Department of Control and Automation Engineering, Electrical-Electronics Engineering Faculty, Yıldız Technical University, İstanbul-TURKEY*
e-mail: gulez@yildiz.edu.tr
[3]*Department of Electrical Engineering, Electrical-Electronics Engineering Faculty, Yıldız Technical University, İstanbul-TURKEY*
e-mail: skoroglu@yildiz.edu.tr

Abstract

In this work, the low frequency electromagnetic emission from permanent magnet synchronous motors is studied. The main objective is to provide a safety region for humans in the vicinity of these motors, especially as these motors are now being used widely in inhabited areas, where high flux densities are expected. In this study, a new proposed equivalent magnetic circuit is used to estimate the stray fields at the surface of the motor. The analysis showed that the emission of the stray field in the radial direction depends on the permeability of the stator body. Low values of permeability may result in very high stray flux emissions with levels that require shielding to protect people in the surrounding areas. Relatively far away from the stator (e.g. 50 cm for the tested motor), the flux is normally at a low level and should not pose a threat to life.

The traced waveforms of the magnetic field showed that waveforms similar to the heartbeat may result, which constitutes a threat to people with pacemakers. In addition, the traced waveform of the x-sensor (radial component) provided important information that could be used to estimate the rotor position of the motor.

Key Words: *Magnetic field measurement, permanent magnet synchronous motor, stray electromagnetic field, magnetic exposure, rotor position*

1. Introduction

Nowadays, relatively large magnetic fields produced by electrical motors such as induction motors, permanent magnet DC motors, and permanent magnet synchronous motors (PMSM) are widely used in inhabited areas, especially in home appliances and electrical vehicles. In electrical vehicles, for example, the motors are generally positioned just under the passenger seats, which expose the passengers to the risk of power frequency magnetic fields (PFMF), as well as to high frequency components generated due to the existence of high current switching

inverters (almost 50 A). For human bioelectronics equipment such as pacemakers [1, 2], this is a very dangerous situation that may be life-threatening.

For biological effects, the responses to low frequency have been categorized into 3 groups [1]: cancer initiation, induced electric fields/currents on body tissues, and disruption of hormonal and immune system mechanisms following inhibition of the activity of the pineal gland. Though the response of biological systems to PFMF is still unclear, a value of 0.20 μT (2 mG) of magnetic flux density has been defined as a safety threshold for exposure of the whole body to PFMF [3]. However, based on epidemiologic studies [4] and 2 pooled analyses [5, 6], PFMF has been classified as a possible human carcinogen by the International Agency for Research on Cancer [7]. In addition, it has been stated that exposure to PFMF of greater than 0.4 μT (4 mG) is considered as a possible cause of childhood leukemia [4, 7], and a low frequency magnetic flux density of only 0.2 μT has been determined as the security limit in incubators for infants [3, 8, 9]. It has also been reported in [10] that if pineal gland secretion, which produces the melatonin hormone in the human body, is subjected to PFMF in the range of 1-100 μT, it may be affected, leading to the changing of the immunological response to infection [3, 11]. Thus, in several applications, such as ship propulsion systems, small amplitude flux densities such as 2.5 μT (25 mG) at 50 cm from the stator of the motor should not be neglected [12]. On the other hand, the shape of the magnetic field density, if properly measured, may hold very important information about the rotor position, which can be used in the PMSM motor control systems. Thus, knowledge about the electromagnetic stray fields of electrical machines is required.

In the literature, a few research efforts have been made [12-16] to measure the magnetic fields around electrical machines with different degrees of success. In [12], the effort was directed to measure the stray magnetic fields necessary to develop a model to represent the stray field outside the induction motor; 3D magnetic sensors were used to measure the induced voltage due to the magnetic field distribution. In [13], measuring techniques were described and an evaluation method to characterize the generated fields was carried out. However, no analytical analysis was carried out, and the results provided did not take the symmetry around the motors into consideration. In [14], the evaluation of the electromagnetic emissions in the high frequency range (100 kHz to MHz level) from large power electrical rotating machinery was considered, and it was reported that emissions are correlated with the operating conditions and the characteristics of the machine under test. In [15-16], the standard limits for electromagnetic and electrical field emissions around human areas were provided. However, no research efforts were devoted to the study of PMSMs as a source of PFMF.

In this study, the objective was to obtain a model capable of estimating the stray magnet field outside the motor, as well as to obtain good knowledge of PMSMs' stray magnetic fields. This knowledge may help in providing technical solutions to reduce stray fields, as well as in designing appropriate electromagnetic shields.

2. Analysis of Stray Magnetic Fields in PMSM

In electrical machines, the air gap flux is produced as an interaction of the rotor magnetic flux and the stator magnetic flux. These variable magnetic fluxes, which have both amplitude and direction varying with time, can be produced by alternating current excitation or by rotation of a permanent magnet attached to the rotor. The net flux produced to the air gap is normally less than the flux produced in the motor due to many losses, such as stray flux, fringing flux, or magnetomotive force (MMF) drop due to reluctances of the magnetic path. In the following section, an analysis leading to estimation of the stray magnetic fields at the surface surrounding

the motor will be discussed.

2.1. PMSM equivalent magnetic circuit

Regarding the permanent magnet as a flux source, the stray magnetic field from the motor can be included in the magnetic circuit of the motor. The possible flux paths of an 8-pole motor are shown in Figure 1.

In Figure 1, the shown flux paths can be explained as follows:

Ψ_{Main} is the main flux linking the stator and the rotor without leakage,

Ψ_{Lr} is the leakage flux from the rotor that fails to link the stator winding,

Ψ_{Ls} is the leakage flux from the stator windings that fails to cross the air gap to link the rotor,

Ψ_{Stray} is part of the main flux that links the stator and the rotor but leaks outside the stator surface, and

Ψ_{airgap} is the air gap flux.

These fluxes, together with their magnetic path properties, can be represented by the equivalent circuit shown in Figure 2.

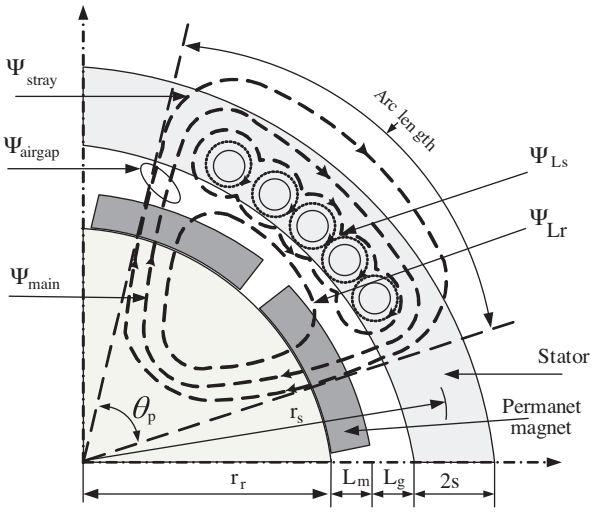

Figure 1. Possible flux paths of an 8-pole PMSM.

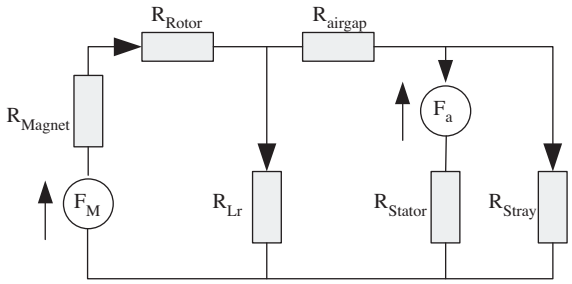

Figure 2. PMSM equivalent magnetic circuit.

Here, F_a is the armature MMF due to stator currents and F_M is the equivalent MMF of the magnets. R_{Lr} leakage reactance due to the leakage flux Ψ_{Lr}

The magnet, the rotor, and the stator reluctances depend on the structure and material properties used to build these components. Generally, the reluctances shown in Figure 2 can be expressed as:

$$\Re_{Magnet} = \frac{\ell_{Magnet}}{\mu_0 \mu_{Magnet} A_{Magnet}}, \tag{1}$$

$$\Re_{Rotor} = \frac{\ell_{Rotor}}{\mu_0 \mu_{Rotor} A_{Rotor}}, \tag{2}$$

$$\Re_{Airgap} = \frac{\ell_{Airgap}}{\mu_0 \mu_{Airgap} A_{Airgap}}, \tag{3}$$

$$\Re_{Stator} = \frac{\ell_{Stator}}{\mu_0 \mu_{Stator} A_{Stator}}, \tag{4}$$

$$\Re_{Stray} = \frac{\ell_{Stray}}{\mu_0 A_{Stray}}. \tag{5}$$

The reluctance due to stray flux Ψ_{Ls} is not shown; however, it originates around the stator windings and its leakage path consists of part of the stator body, the slot structure path, and part of the air gap. This flux normally does not leak outside the motor.

The cross section area associated with these reluctances can generally be expressed as:

$$A_{Magnet} < A_{Rotor} < A_{Gap} < A_{Stator} < A_{Stray},$$

where l stands for the flux path length, A stands for the cross section area taken at the mean radius of the corresponding section, and μ stands for the relative permeability.

2.2. Estimation of the stray magnetic fields

For PMSM, the existence of strong magnet bars, such as samarium-neodymium, produces a high magnetic density in the air gap (up to 1 T). When the motor rotates, alternating magnetic fields are generated with a frequency corresponding to the motor speed and the number of pole pairs. The leaking of this magnetic field results in stray magnetic fields around the motor. These stray fields, at a few centimeters (up to 20 cm) from the surface of the motor, can be estimated in the radial direction as follows.

Assuming that the air gap flux per pole is known and that initially $\mathrm{F}_a = 0$, the flux crossing the air gap will be divided between the stator body and the stray path according to

$$\psi_{Stray} = \frac{\Re_{Stator}}{\Re_{Stator} + \Re_{Stray}} \psi_{airgap}, \tag{6}$$

where R_{Stator} is the stator reluctance given in equation (4) due to stator yoke and stator teeth. Assuming that the path of the flux is uniform, then the stator flux path length l_{Stator} can be roughly estimated as:

$$l_{\mathrm{Stator}} = \text{ stator thickness + stator pole arc length } = 2S + 2\pi r_s \theta_p,$$

where θ_p is the pole angle (as a fraction of the complete circle). Therefore,

$$\Re_{Stator} = \frac{2S + 2\pi r_s \theta_p}{\mu_0 \mu_{Stator} (2\pi r_s \theta_p L_{Stack})}, \tag{7}$$

where L_{Stack} is the stack length.

Similarly, the stray reluctance at x meters from the stator surface can be calculated as

$$\Re_{Stray} = \frac{2x + 2\pi(r_s + s + x)\theta_p}{\mu_0 (2\pi(r_s + s + x)\theta_p L_{Stack})}. \tag{8}$$

Inserting equations (7) and (8) into equation (6) results in:

$$\psi_{Stray} = \frac{1}{1 + \left(\frac{x+\pi(r_s+s+x)\theta_p}{r_s+s+x}\right)\left(\frac{r_s \mu_{Stator}}{s+\pi r_s.\theta_p}\right)} \Psi_{Airgap}. \tag{9}$$

In terms of magnetic flux density, this can be written as

$$B_{Stray} = \frac{1}{1 + \left(\frac{x+\pi(r_s+s+x)\theta_p}{r_s+s+x}\right)\left(\frac{r_s\mu_{Stator}}{s+\pi r_s.\theta_p}\right)} B_{Airgap}\left(\frac{r_s - s}{r_s + s + x}\right). \tag{10}$$

3. Measurement and Experimental Results

3.1. Measurement setup

Two different measurement setups were used to study the stray magnetic field around the motor. The first setup was composed of a commercial Gauss meter, which gives the net flux density at the selected points. The second setup was composed of simple and direct visible measurements developed specially to measure the alternating magnetic field density originating from rotating electrical machines and power lines. The block diagram of this measuring setup is shown in Figure 3a. It is composed of 3 air core-based orthogonal magnetic coils used as sensors. The air core is used to avoid disturbance of the magnetic field distribution.

Ignoring the saturation resistors in Figure 3b, the measured signal can be expressed as

$$\begin{aligned} \text{Measured Signall} &= -\tfrac{1}{R_2C}\int E_{out}dt \\ &= \tfrac{R_fNA}{R_1R_2C}\int dB = \tfrac{R_fNA}{R_1R_2C}B \\ &= kB \end{aligned} \tag{11}$$

where E_{out} is the amplified induced voltage in the coil, N is the coil's number of turns; and A is the coil cross section area.

From equation (12), it can be seen that the measured signal is directly proportional to the number of turns as well as to the cross section area. For the fractional error in turns, the number ΔN, the error in the measured signal, is in the order of $\Delta N/N$; therefore, for a large number of turns, the sensitivity of the measured signal to errors in number of turns can be ignored. However, since for compact systems it is preferable to have small cross section areas, the sensitivity of the measured signal is directly proportional to the errors in the cross section area. As a result, the sensitivity to both errors in number of turns and cross section area can be expressed as:

$$\text{Errors in measurement } = (\Delta N/N + \Delta A/A) * kB. \tag{12}$$

The dimensions of the coils are as follows: number of turns = 200; apparent cross section area = 19.6 mm^2, and captured flux area = 1590 mm^2. The output of the sensors is connected to a signal conditioning circuit composed of an amplifier circuit followed by an integrator. The output of the integrator is connected directly to an oscilloscope to observe the measured shape of the magnetic flux. It should be noted that the output of the integrator, as shown in Figure 3b, can also be connected to a digital calculating block to measure the net magnetic flux, or may be used as a control signal for active shielding. This simple measuring interface photo is shown in Figure 3c.

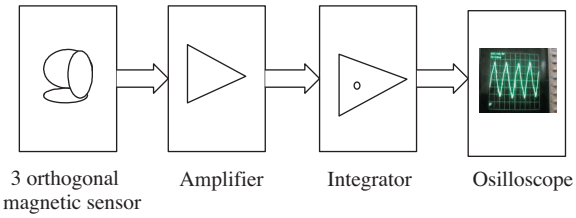

Figure 3a. Block diagram of the measuring system.

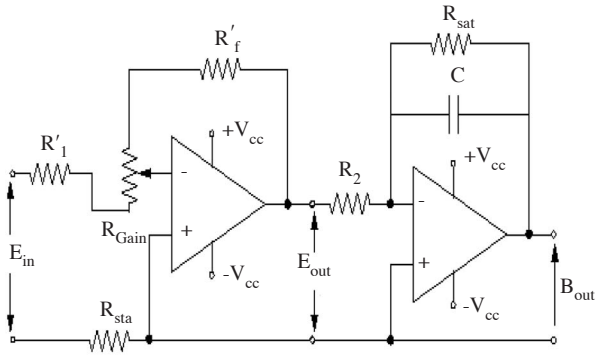

Figure 3b. Amplifier and integrator stage.

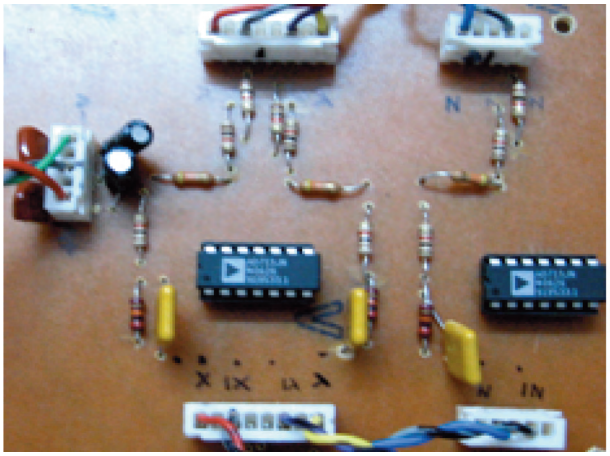

Figure 3c. Photo of the signal conditioning stage.

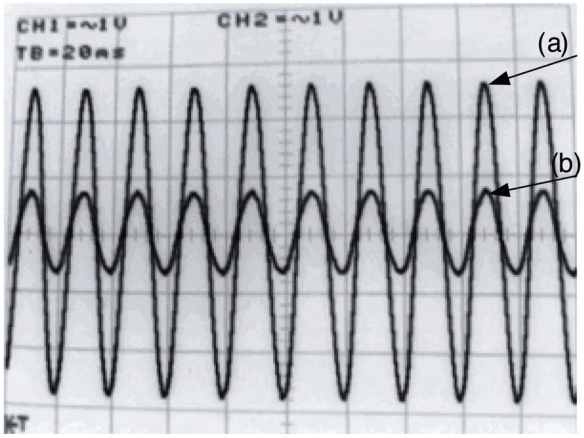

Figure 3d. Magnetic field density sensed at 20 cm from a 3-phase bar carrying 500 A, (a) without shield and (b) with shielding, 1 mV $\equiv$ 1.5 mG.

Examples of different measured magnetic field signals achieved with this arrangement are shown in Figures 3d and 3e.

Figure 3d shows the measured magnetic field density sensed at 20 cm from the 3-phase bar carrying 500 A. This figure consists of 2 measured signals to the same source, one (a) without a shield and the other (b) with shielding. The shielding characteristic consists of cylindrical-shaped transformer grade iron with electrical conductivity equal to 2.17×10^6 S/m and magnetic permeability equal to 4000; more detailed information is in [17]. Figure 3e shows an example of measured magnetic field density sensed at 10 cm from a 4-pole permanent magnet DC machine.

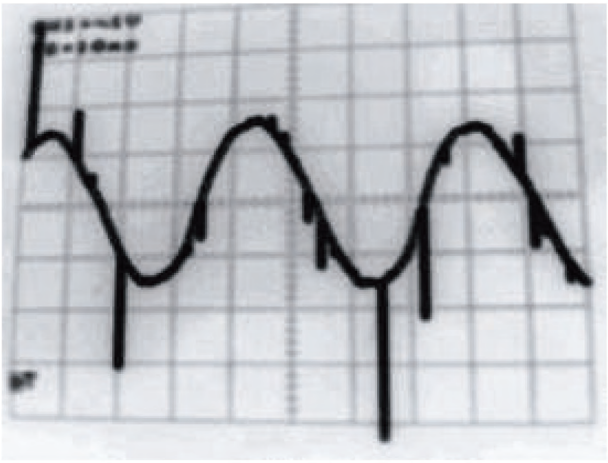

Figure 3e. Magnetic field density waveform sensed at 10 cm from a 4-pole permanent magnet DC machine rotating at 1000 rpm, 1 mV $\equiv$ 1.5 mG.

It should be noted that the measured signal was very weak and could easily be affected by the surrounding noises. For the inverter system driving the PMSM, there are wide ranges of noises, extending from switching noises to generated EMI noises. These noises appear in the measured signal as sharp pulses, as shown in Figure 3e. Therefore, the final design should be protected against such noises by using EMI filters for a certain range of measuring frequencies.

3.2. Experimental setup and results

In Figure 4, the experimental setup shows the PMSM and the zero level measured flux points, which are just above the motor. The motor, which is positioned in the middle of a cubic measuring cage, is driven with an IGBT inverter under a direct torque control algorithm. The motor parameters are shown in the Table. The distance between the motor and the control system is taken as sufficiently large to neglect the interaction of its field. The flux density is measured around the motor at the designated points at 2 different levels with a standard Gauss meter that gives the net value of the flux density.

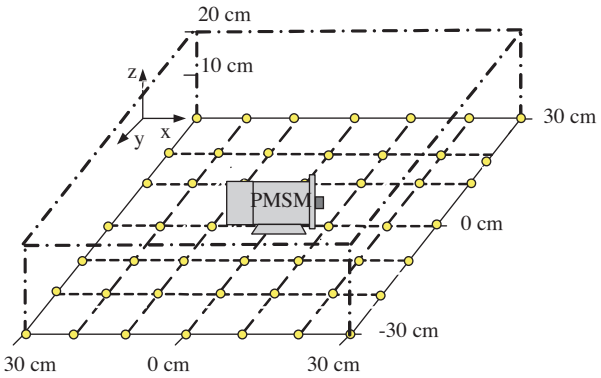

Figure 4. Experimental setup shows the PMSM and points of measurement.

The results of the measurements were plotted in 3D figures for 2 different levels above the motor to inspect the stray field distribution. The flux performance at z = 10 cm above the motor is shown in Figure 5, while the performance at z = 20 cm above the motor is shown in Figure 6. The figures show the variation of the field with horizontal distance from the motor. It is clear from the Figures that the flux density rapidly decreased with the increasing of distance from the motor. The contours show that the resulting magnetic flux density was smaller at the axial directions (x- in Figure 4), compared with the radial direction. It is seen that this was an expected result, since the rotating motor flux is normally designed to be in the radial direction. However, due to the end windings and the nature of the magnetic field distributions in the air, the field also existed with a different waveform in the axial directions.

Table. Technical data of the MMD082A PMSM used in the experiments.

Rated output	0.750 kW
Number of poles	8
Rated speed	3000 rpm
Rated torque	2.4 Nm
Rated current	4.3 A (rms)
Supply voltage (AC)	200 V
Electrical Time constant L/R	7.4 ms
Voltage constant per phase	$21.4e^{-3}$ V(rms)/min^{-1}
Excitation Voltage constant	$45.3e^{-3}$ V(0-p)/min^{-1}
Torque constant	0.61 Nm/Amp (rms)
Flux per pole	72.25 mWeber
μ_{stator}	2000
r_s	4 cm
s	1 cm

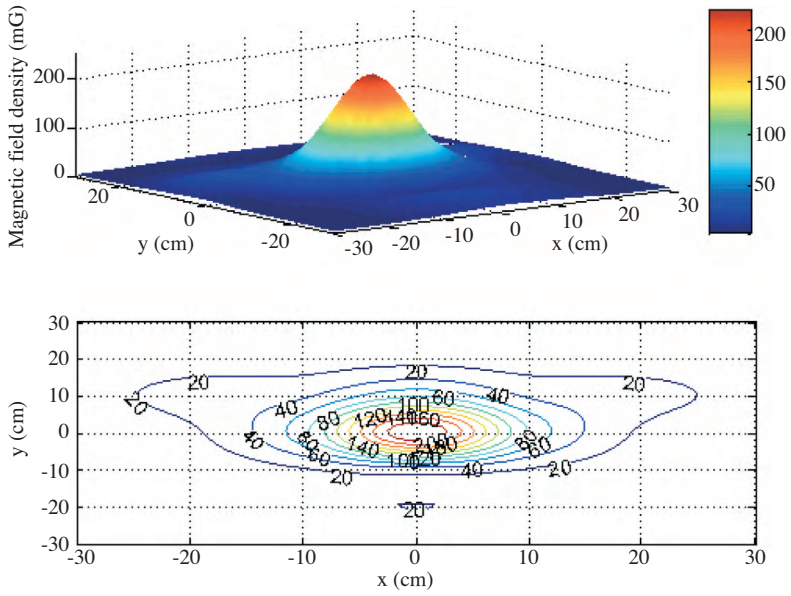

Figure 5. 3D map (upper) and its contours (lower) showing the distribution of the magnetic field density at z = 10 cm above the motor (line voltage, 54 V; rotor speed, 900 rpm).

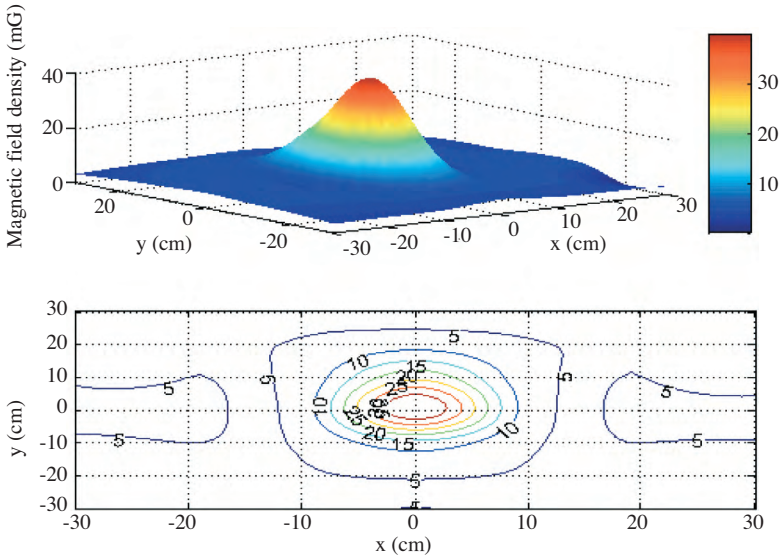

Figure 6. 3D map (upper) and its contours (lower) showing the distribution of the magnetic field density at z = 20 cm above the motor (line voltage, 54 V; rotor speed, 900 rpm).

The variation of the magnetic field with distance, measured at the points above the middle of the motor as shown in Figure 7, is plotted with logarithmic scale in Figure 8. Near the motor body (2 cm), a higher field density of as much as 512 mG was recorded. The magnitude of the flux density decreased quickly with an increase in the measured distance, to less than 10 mG at 50 cm from the motor surface.

Figure 8 also shows the estimated flux density calculated with equation (10); the motor parameters are given in the Table, with the operating rotor speed equal to 900 rpm. It can be observed from the comparison of the 2 curves that they were almost the same near the motor region up to 20 cm; however, when the distance increased, they gradually parted. Thus, the developed equations (or model) can roughly be used to estimate the stray magnetic flux density around the motor up to a few centimeters. Away from the motor, the figure shows that the flux density decreases quickly, according to the inverse square law.

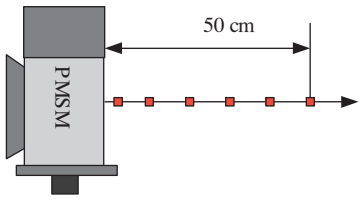

Figure 7. Points of measurement in the radial direction above the middle of the motor.

3.3. The shape of the magnetic field waveform

The measuring system shown in Figure 3 was used to trace the actual waveform of the stray magnetic field from the motor; the coil sensor set was positioned at 5 cm away from the stator surface, as shown in Figure 9. The traced x-sensor flux density was a sinusoidal waveform with an amplitude of 150 mG and some pulse harmonics due to inverter switching, as in Figure 10a. This flux was indeed a combination of the flux due to

the permanent magnet rotation and the flux due to the stator winding currents. The traced y-sensor in Figure 10b describes a sinusoidal waveform, as well, with a relatively smaller amplitude (75 mG). On the other hand, the traced z-sensor flux density was the smallest; in addition, the waveform was full of pulse harmonics and oscillated with a different frequency. The combinations of such harmonics may result in a waveform similar to a heartbeat (Figure 10c), which may interfere with pacemakers and similar devices. The combination of the 3 components, in fact, describes the shape of propagation of the magnetic field in the region around the motor.

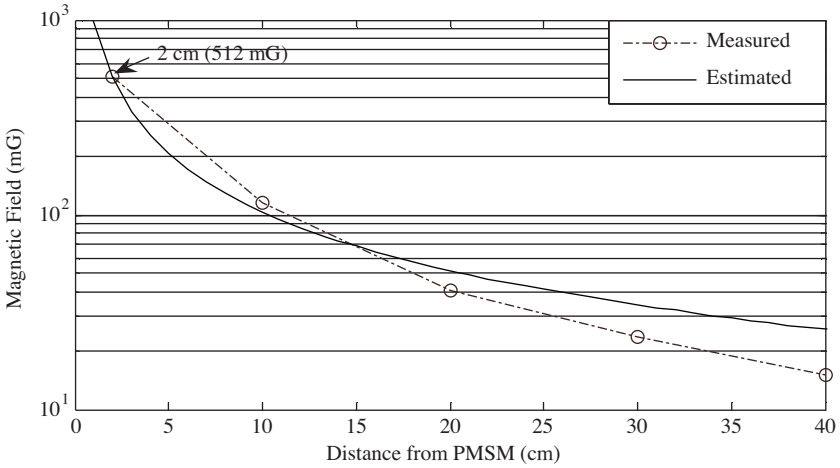

Figure 8. Flux density measured and estimated with equation (10) above the middle of the motor.

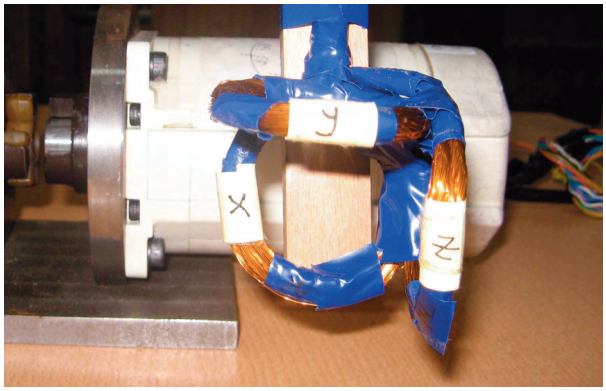

Figure 9. The 3 orthogonal air coil sensors measuring the flux density leaking from the PMSM.

In a PMSM, the measurement of the rotor angle is very important for achieving accurate torque or speed control. The measured rotor position is normally used to calculate the motor's instantaneous flux and torque values, as well as to achieve the axis transformation necessary for the control system. This angle is normally measured with hall sensors, or is sometimes inaccurately estimated from the measured motor currents. In Figures 11 and 12, the traced flux waveform for the x-sensor and y-sensor with the instantaneous phase A current are shown, respectively. It is clear that the flux waveform and the current waveform were oscillating together with a small phase difference. Bearing in mind that the rotor position was almost identical to the radial flux distribution and that the flux waveform was smoother than the pulsed current waveform due to inverter switching, the accurate measurement of the radial flux component could lead to an accurate estimation of the rotor position.

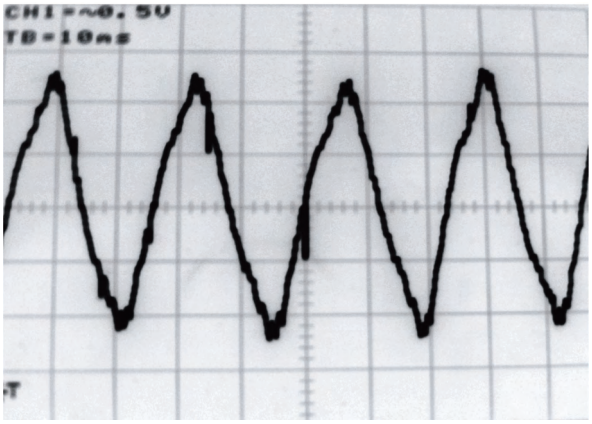

Figure 10a. The magnetic flux density traced with the x-sensor (CH 1 = ∼0.5 V, TB = 10 ms, 1 mV ≡ 3/2 mG).

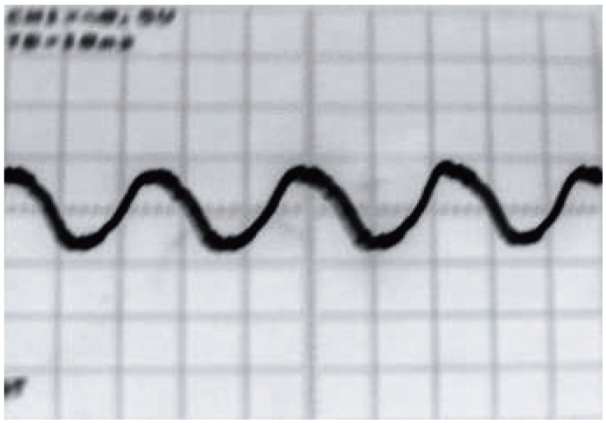

Figure 10b. The magnetic flux density traced with the y-sensor (CH 1 = ∼0.5 V, TB = 10 ms, 1 mV ≡ 3/2 mG).

Figure 10c. The magnetic flux density traced with the z-sensor (CH 1 = ∼0.5 V, TB = 10 ms, 1 mV ≡ 3/2 mG).

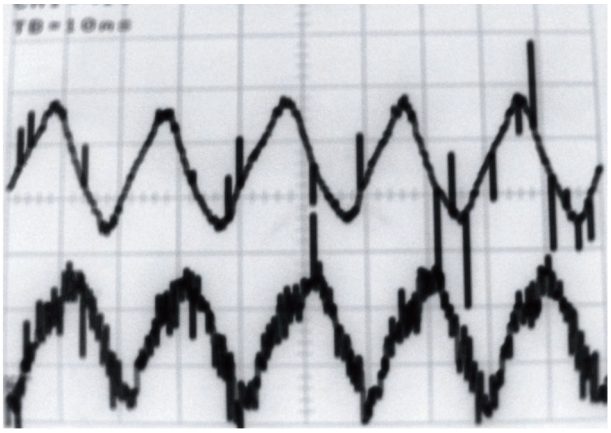

Figure 11. Instantaneous flux of the x-sensor (upper; CH 1 = ∼0.5 V, TB = 10 ms, 1 mV ≡ 3/2 mG) and phase A current (lower; CH 2 = ∼1 V, TB = 10 ms).

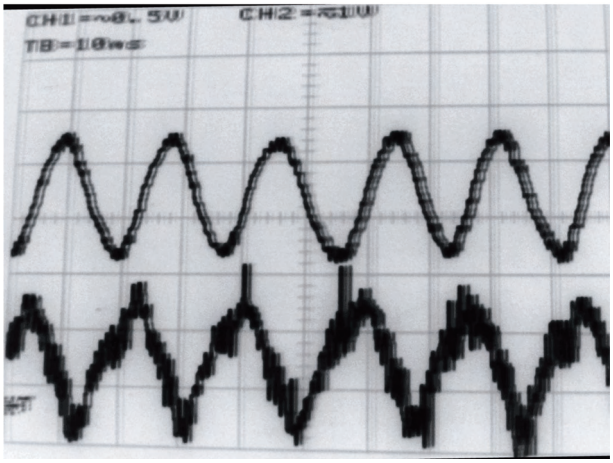

Figure 12. Instantaneous flux density of the y-sensor (upper; CH 1 = ∼0.5 V, TB = 10 ms, 1 mV ≡ 3/2 mG) and phase A current (lower; CH 2 = ∼1 V, TB = 10 ms).

4. Conclusions

In this work, the low frequency electromagnetic emission from a PMSM is studied. The main objective was to provide safety regions for humans in the vicinity of these motors, especially in electrical vehicles where high current and hence high flux density emissions are expected. A new proposed equivalent magnetic circuit is used to estimate the stray fields from the PMSM. It was shown by analysis that the emission of the stray field in the radial directions depended on the permeability of the stator body. Low values of this parameter may result in very high stray flux emissions at levels that may require shielding of the motor. Relatively far away from the stator, the flux is normally of a small level and may not represent an exposure threat.

The traced z-sensor showed that waveforms similar to the heartbeat may result, which may interfere with pacemaker operating mechanisms; therefore, wearers of cardiac pacemakers should not be exposed to high power frequency fields.

The traced waveform of the x-sensor (radial component) provided important information that could be used to estimate rotor position.

References

[1] J.R. Ashley, B. Myers, H.C. Lilly, R.E. Beatie, "Measurement of potential magnetic field interference with implanted cardioverter defibrillators or pacemakers", Electro 98 Professional Program Proceedings, pp. 159–170, 1998.

[2] American Conference of Governmental Industrial Hygienists, "Documentation of the threshold limit values for physical agents in the work environment," ACGIH, Cincinnati, 1995.

[3] N. Petrucci, "Exposure of the critically ill patient to extremely low-frequency electromagnetic fields in the intensive care environment", Intensive Care Med., Vol. 25, pp. 847–851, 1999.

[4] C.Y. Li, G. Mezei, F.C. Sung, M. Silva, P.C. Chen, P.C Lee, L.M. Chen, "Survey of residential extremely-low-frequency magnetic field exposure among children in Taiwan", Environment International, Vol. 33, pp. 233–238, 2007.

[5] A. Ahlbom, N. Day, M. Feychting, E. Roman, J. Skinner, J. Dockerty et al. "A pooled analysis of magnetic fields and childhood leukemia", Br. J. Cancer, Vol. 83, pp. 692–8, 2000.

[6] S. Greenland, A.R. Sheppard, W.T. Kaune, C. Poole, M. Kelsh. "A pooled analysis of magnetic fields, wire codes, and childhood leukemia", Epidemiology, Vol. 11, pp. 624–34, 2001.

[7] International Agency for Research on Cancer (IARC), "IARC monographs on the evaluation of carcinogenic risks to humans", Vol. 80, Lyon: IARC, 2001.

[8] C.F. Bearer, "Electromagnetic field and infant incubator", Arch. Environ. Health, Vol. 49, pp. 352–354, 1994.

[9] S.E. Aasen, A. Johnsson, D. Bratlid, T. Christensen, "Fifty-hertz magnetic field exposure of premature infants in a neonatal intensive care unit", Biol. Neonate, Vol. 70, pp 249–264, 1996.

[10] B.W. Wilson, R.G. Stevens, L.E. Anderson, "Neuroendocrine mediated effects of electromagnetic fields exposure: possible role of the pineal gland", Life Sci., Vol. 45, pp. 1319–1332, 1989.

[11] R.J. Reiter, "The pineal gland and melatonin in relation to aging: a summary of the theories and of the data", Exp. Gerontol., Vol. 30, pp. 199–212, 1995.

[12] G. Le Coat, A. Foggia, J.P. Bongiraud, and P. Le Thiec, "Electromagnetic signature of induction machines", IEEE Transactions on Energy Conversion, Vol. 14, pp. 628–632, 1999.

[13] G.G. Karady, Sh.H. Berisha, M. Muralidhar, J.A. Demcko, M. Samotoy, "Variable speed motor drive generated magnetic fields", IEEE Transactions on Power Delivery, Vol. 9, pp. 1639–1646, 1994.

[14] P. Ferrari, A. Mariscotti, A. Motta, P. Pozzobon, "Electromagnetic emissions from electrical rotating machinery", IEEE Trans. on Energy Conv., Vol. 16, pp. 68–73, 2001.

[15] IEEE Standard 644-1994, "IEEE standard procedures for measurement of power frequency electric and magnetic fields from AC power lines", 7 March 1995.

[16] IEEE Standard 291-1991, "IEEE standard methods for measuring electromagnetic field strength of sinusoidal continuous waves, 30 Hz to 30 GHz", 23 August 1991.

[17] N. Umurkan, S. Koroglu, O. Kilic, A.A. Adam, "A neural network based estimation method for magnetic shielding at extremely low frequencies", Expert Systems with Applications, Vol. 37, pp. 3195–3201, 2010.